Implementation of a Frenkel exciton-based controlled phase shifter

Bernard Yurke,[1,*] Richard Elliott,[1] and Aaron Sup[2]
[1]*Micron School of Materials Science and Engineering, Boise State University, Boise, Idaho 83725-1320, USA*
[2]*Department of Physics, Boise State University, Boise, Idaho 83725-1320, USA*

(Received 31 August 2022; accepted 16 December 2022; published 4 January 2023)

Frenkel excitons are of interest for ultrafast switching applications due to the femtosecond timescale at which coherent exciton transfer between chromophores takes place. The Frenkel Hamiltonian, which governs the dynamics of Frenkel excitons, belongs to a class of Hamiltonians that enable universal quantum computation. It is thus of interest to determine how a complete set of exciton-based gates for quantum computing could be constructed as aggregates of chromophores. We demonstrate that a controlled phase shifter can be constructed as a pair of exciton transmission lines that employ two types of chromophores and that are cross coupled by a two-exciton interaction. This element facilitates the construction of controlled basis-change gates, thereby enabling the implementation of a complete set of exciton-based gates for universal quantum computation.

DOI: 10.1103/PhysRevA.107.012603

I. INTRODUCTION

The control that DNA-based self-assembly [1,2] affords in assembling chromophores, generally consisting of the optically active component of organic dyes, into complex well-defined structures [3–5] has led to interest in the use of this technology to form chromophore aggregates that function as coherent exciton-based devices [6–11] and potentially for quantum computing [12,13]. These excitons consist of the quantum of energy that is required to induce a transition from the ground electronic state of a chromophore to its lowest optically allowed excited state. These are referred to as Frenkel excitons and have dynamics governed by the Frenkel Hamiltonian. In an aggregate of chromophores, this energy acts as a quasiparticle such that it will propagate coherently throughout the aggregate, mediated by Coulomb interactions that induce one chromophore to deexcite while a neighboring chromophore is excited. This coupling is often approximated as the dipole-dipole coupling between the transition dipoles of a pair of chromophores and is modeled as an excitonic hopping interaction [14].

Frenkel excitons also exhibit exciton-exciton interactions. These can arise via two mechanisms. The first is the result of the energy deficit or excess when the molecule is doubly excited compared to that of two singly excited molecules. This represents the energy cost of having two excitons occupy the same chromophore [15]. This interaction is modeled by anharmonicity terms in the Frenkel Hamiltonian. The second mechanism gives rise to an interaction between excitons residing on neighboring chromophores. This Coulombic interaction arises from the difference between the static (permanent) charge distribution of a molecule in its ground electronic state and its lowest excited state. This interaction is often approximated as dipole-dipole coupling between dipoles [14] whose moments consist of the difference between the ground-state and lowest excited-state static dipole moments, hereafter referred to as a difference static dipole moment.

The Frenkel Hamiltonian, consisting of a sum of hopping Hamiltonians that transfer quasiparticles between sites and one-site and two-site two-particle-interaction Hamiltonians, belongs to a class of Hamiltonians with which universal quantum computation can be implemented as a many-particle quantum walk [16] provided the two-particle interactions are of suitable form. It is thus of interest whether the exciton-exciton interactions realizable in chromophore aggregates enable the implementation a complete set of gates required for universal quantum computation. Here we show this is the case.

Following Childs *et al.* [16], a many-particle quantum-walk architecture is adopted in which arrays of closely placed chromophores function as exciton wires (transmission lines) connecting gates. We adopt a dual-rail representation in which a qubit is carried by a pair of transmission lines as an exciton wave packet that consists of a superposition state in which the exciton resides on either of the transmission lines. The qubit codes the quantum-mechanical amplitudes with which the exciton resides on either of the transmission-line pairs. In this implementation, basis-change gates are easily formed by bringing the two wires in close proximity at the gate location such that the exciton can hop from one transmission line to the other. This gate can be viewed as the exciton equivalent of an optical beam splitter. The design of such gates has been discussed by Yurke and Kuang [17]. In principle, any desired coupling (basis-change transformation) can be realized through proper choice of the hopping interaction strengths between pairs of chromophores in the gate and achieved by proper adjustment of the spacing between chromophores.

Phase gates are also easily implemented as propagation delays which can be realized by either adjusting the lengths

*Also at Department of Electrical and Computer Engineering, Boise State University, Boise, ID 83725-1320, USA.

of the wire assemblies or inserting a section of transmission line with chromophores whose optical transition frequency is shifted. The optical transition frequencies of chromophores can be modified by changing substituents, thereby enabling the synthesis of chromophores with suitable optical transition frequency. It is also noted that a basis-change gate can function as a phase shifter if two of the ports are terminated with properly chosen chromophores [17].

To complete the list of gates needed for universal quantum computation, a gate is required in which the propagation of one exciton is altered by the presence of a second exciton. In the dual-rail implementation this is achieved by bringing a pair of transmission lines carrying one qubit in the vicinity of a pair of transmission lines carrying a second qubit such that the excitons can interact via a two-body interaction. This must be done in such a way that excitons are prevented from hopping between transmission-line pairs. We show that this can be achieved by employing two types of chromophores, one for which the transition dipole and difference static dipole are parallel and the other for which the transition dipole and difference static dipole are perpendicular. Because in the dual-rail architecture each exciton always resides on its dedicated pair of transmission lines as it ballistically propagates through the gate network, each exciton can be regarded as a distinguishable particle. Childs *et al.* [16] have shown that a controlled phase shifter can be implemented with distinguishable particles provided the Hubbard interaction is of a two-δ-function type. We show that such a two-exciton interaction can be implemented by judiciously placing and orienting the two types of chromophores along two neighboring transmission lines. A controlled basis change gate, of which a controlled-NOT (CNOT) gate is an example, can be implemented by sandwiching the controlled phase shifter between a pair of basis-change gates along the path of the target qubit (as opposed to the control qubit). This completes the set of gates needed for universal quantum computation.

The implementation of a full set of gates for universal quantum computation as suitably constructed chromophore aggregates shows the potential utility of such aggregates for information processing, especially when ultrafast switching is desired, as exciton hopping between chromophores occurs on femtosecond timescales. That scalable quantum computation can be realized with such aggregates is however in doubt due to loss of coherence by dephasing that results from the coupling between the vibrations and the electronic degrees of freedom of a chromophore [18]. The degree to which this can be mitigated by chromophore design or by low-temperature operation remains to be seen.

Because photons are converted into excitons and vice versa by absorption and emission, exciton-based switches may have applications in nonlinear and quantum optics as well. In this regard, the controlled phase shifter can be regarded as a nonlinear Kerr medium capable of producing large phase shifts at the single-photon level.

II. FRENKEL EXCITON THEORY

The Frenkel exciton Hamiltonian has the general form [14,15]

$$H = \sum_r \epsilon_r B_r^\dagger B_r + \sum_{(r,s)} J_{r,s}(B_r^\dagger B_s + B_s^\dagger B_r) + \sum_r \frac{\Delta_r}{2} B_r^\dagger B_r^\dagger B_r B_r + \sum_{(r,s)} K_{r,s} B_r^\dagger B_s^\dagger B_s B_r, \tag{1}$$

where B_r is the annihilation operator for an exciton on site (chromophore) r. The exciton creation and annihilation operators satisfy the usual Boson commutation relations. The prefactor ϵ_r is the optical transition energy of a chromophore indexed by r and Δ_r is the anharmonicity parameter. The (r, s) indices indicate summation over all distinct site (chromophore) pairs. Further, $J_{r,s}$ denotes the exciton hopping energy or exchange energy. This energy is often approximated as the dipole-dipole interaction [14] between transition dipoles,

$$J_{r,s} = \frac{\mu_r \mu_s}{4\pi\epsilon R_{r,s}^3}[\mathbf{n}_r \cdot \mathbf{n}_s - 3(\mathbf{n}_{r,s} \cdot \mathbf{n}_r)(\mathbf{n}_{r,s} \cdot \mathbf{n}_s)], \tag{2}$$

where μ_r and $\mathbf{n}_r$ are the magnitude and the orientation vector, respectively, of the transition dipole r, $R_{r,s}$ is the distance between the dipoles, and $\mathbf{n}_{r,s}$ is the unit vector that lies parallel to the line joining the centers of the two chromophores. In addition, $K_{r,s}$ is the interaction energy between a pair of excitons with one residing on chromophore r and the other on chromophore s. This energy is also often approximated as an interaction [14] between point dipoles,

$$K_{r,s} = \frac{\Delta d_r \Delta d_s}{4\pi\epsilon R_{r,s}^3}[\mathbf{m}_r \cdot \mathbf{m}_s - 3(\mathbf{n}_{r,s} \cdot \mathbf{m}_r)(\mathbf{n}_{r,s} \cdot \mathbf{m}_s)], \tag{3}$$

where Δd_r and $\mathbf{m}_r$ are the magnitude and orientation vector, respectively, for the difference static dipole at site r. Note that the orientation vector $\mathbf{n}_r$ for the transition dipole need not be parallel to the orientation vector $\mathbf{m}_r$ for the difference static dipole [19], a fact we exploit in constructing the controlled phase shifter.

III. CONTROLLED PHASE SHIFTER

We now consider two parallel transmission lines, of the same periodicity, and restrict our attention to the case in which at most one exciton resides on each transmission line. The transmission lines are taken to be engineered to prevent exciton hopping from one transmission line to the other, in which case the only coupling between the transmission lines is that of the two-body interaction $K_{r,s}$. In this case, the one-site exciton-exciton interaction term of the Hamiltonian, characterized by the energy Δ_r of Eq. (1), is zero and is now dropped. For simplicity, only nearest-neighbor intra-transmission-line exciton exchange interactions are kept. In restricting the Hamiltonian (1) to the present case, it is convenient to express the Hamiltonian as a sum of three

Hamiltonians

$$H = H_A + H_B + H_I, \tag{4}$$

where the Hamiltonian of transmission line A is given by

$$H_A = \hbar\omega_A \sum_{r=-\infty}^{\infty} A_r^\dagger A_r + \hbar\omega_{JA} \sum_{r=-\infty}^{\infty} (A_{r+1}^\dagger A_r + A_r^\dagger A_{r+1}), \tag{5}$$

the Hamiltonian for transmission line B is given by

$$H_B = \hbar\omega_B \sum_{r=-\infty}^{\infty} B_r^\dagger B_r + \hbar\omega_{JB} \sum_{r=-\infty}^{\infty} (B_{r+1}^\dagger B_r + B_r^\dagger B_{r+1}), \tag{6}$$

and the Hamiltonian for the coupling between the transmission lines is given by

$$H_I = \sum_{(r,s)} K_{r,s} A_r^\dagger B_s^\dagger B_s A_r. \tag{7}$$

Here A_r and B_r denote the exciton operators at site r for transmission lines A and B, respectively. Note that Hamiltonians H_A and H_B are invariant under translation by an integer multiple of lattice units.

This pair of transmission lines is operated as a controlled phase shifter by arranging two-exciton wave packets, one on each transmission line, to pass each other. When the wave packets are far apart, the interaction (7) is negligible. During the period when the wave packets overlap, H_I becomes nonnegligible and results in a winding of the overall phase of the system. The controlled phase shifter can be operated in one of two modes: the head-on collision mode in which the wave packets approach each other from opposite directions and the rear-end collision mode in which a wave packet having a greater group velocity overtakes a wave packet having a slower group velocity. For proper operation, exciton backscattering is to be avoided. Because the two excitons reside on separate transmission lines, they can be regarded as distinguishable particles. Childs *et al.* [16] showed that for the case of distinguishable particles backscattering can be avoided if the exciton-exciton interaction $K_{r,s}$ is of the two-δ-function form

$$K_{r,s} = \hbar\omega_I(\delta_{r,s-1} + \delta_{r,s+1}). \tag{8}$$

As such, an exciton on one transmission line interacts with the exciton of the other transmission line at two different sites. This enables destructive interference of the backscattered amplitude resulting from the two sites, thereby suppressing backscattering and enabling forward propagation with the accumulation of a nontrivial phase shift. Note that if only one exciton is present, the interaction described by Eq. (7) is zero and no phase is accumulated from this term of the Hamiltonian. The device thus functions as a controlled phase shifter in that both excitons must be present for the system to accumulate the phase. Also noteworthy is that, with Eq. (8), the total Hamiltonian (4) is translationally invariant under a translation by an integer number of lattice units.

IV. IMPLEMENTATION OF A TWO-δ-FUNCTION EXCITON-EXCITON INTERACTION

A two-transmission-line system, which implements the two-δ-function interaction (8), is shown in Fig. 1. We choose

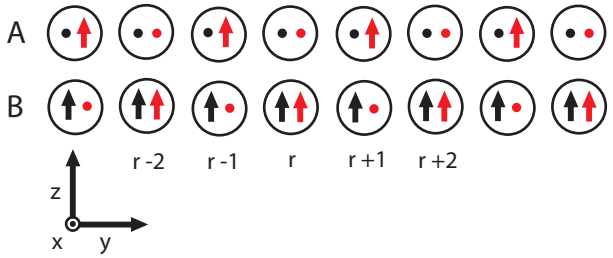

FIG. 1. Two transmission-line system implementing the two-δ-function interaction of Eq. (8). See the text for details.

a coordinate system in which the x axis is perpendicular to the plane of the figure, the y axis runs horizontally, and the z axis runs vertically. The unit vectors parallel to these three axes are denoted by $\mathbf{i}$, $\mathbf{j}$, and $\mathbf{k}$, respectively. Each chromophore is represented as a circle, in which the direction of the transition dipole and the difference static dipole is indicated. A dot represents a dipole pointed in the $\mathbf{i}$ direction and an upward-pointing arrow indicates a dipole pointed in the $\mathbf{k}$ direction. The color of the dot or upward-pointing arrow indicates if the dipole is a transition dipole (black) or a difference static dipole (red). The arrangement of chromophores constituting the upper transmission line A alternates between two chromophore types, one in which the transition and difference static dipoles are parallel and the other in which these two dipoles are orthogonal. The arrangement of chromophores constituting the lower transmission line B also alternates between a chromophore for which the two dipoles are parallel and a dye for which the two dipoles are orthogonal. In its most general implementation, four different chromophores would be employed, two for transmission line A and two for transmission line B.

To avoid band gaps in the dispersion relation for each transmission line, the two chromophores of the upper transmission line should have the same optical transition frequency ω_A. Similarly, the two chromophores of the lower transmission line should have the same optical transition frequency ω_B. Let $\boldsymbol{\mu}_{Ar}$ and $\mathbf{d}_{Ar}$ denote the transition dipole and difference static dipole, respectively, for the chromophore at site r of transmission line A. Similarly, let $\boldsymbol{\mu}_{Br}$ and $\mathbf{d}_{Br}$ denote the transition dipole and difference static dipole, respectively, for the chromophore at site r of transmission line B. To avoid band gaps in the transmission-line dispersion relation the magnitude of the transition dipoles should be the same for the two chromophore types of transmission A and similarly for transmission line B. The transition dipoles are thus given by

$$\boldsymbol{\mu}_{Ar} = \mu_A \mathbf{i}, \tag{9}$$
$$\boldsymbol{\mu}_{Br} = \mu_B \mathbf{k}. \tag{10}$$

The difference static dipoles alternate between even and odd sites and, to avoid spoiling translation invariance of the Hamiltonian under a unit lattice translation, are taken to be

$$\mathbf{d}_{A2r} = d_A \mathbf{i}, \tag{11}$$
$$\mathbf{d}_{B2r} = d_B \mathbf{k}, \tag{12}$$
$$\mathbf{d}_{A2r+1} = d_A \mathbf{k}, \tag{13}$$
$$\mathbf{d}_{B2r+1} = d_B \mathbf{i}. \tag{14}$$

The exciton exchange energies obtained using Eq. (2) and Eqs. (9) and (10) are

$$J_{Ar,As} = \frac{\mu_A^2}{4\pi\epsilon a^3 |r-s|^3}, \tag{15}$$

$$J_{Ar,Bs} = 0, \tag{16}$$

$$J_{Br,Bs} = \frac{\mu_B^2}{4\pi\epsilon a^3 |r-s|^3}, \tag{17}$$

where a is the lattice spacing. Equation (16) shows that no exciton exchange occurs between transmission lines A and B. This is a consequence of choosing the transition dipoles of transmission line A to be orthogonal to those of transmission line B. Equations (15) and (17) show that intratransmission-line exciton-exchange energy is nonzero, enabling excitons to propagate along the transmission lines. The exchange energy falls off as the cube of the distance between sites. By neglecting all but nearest-neighbor coupling, $|r-s| = 1$, one obtains the Hamiltonians of Eqs. (5) and (6).

The exciton-exciton interaction energies obtained using Eqs. (3) and (11)–(14) are

$$K_{r,s} = \frac{d_A d_B}{4\pi\epsilon |(r-s)^2 a^2 + b^2|^{3/2}} F_{r-s}, \tag{18}$$

where

$$F_{r-s} = \begin{cases} 0 & \text{if } r-s \text{ is even} \\ 1 & \text{if } r-s \text{ is odd.} \end{cases} \tag{19}$$

Note that $K_{r,r} = 0$ and the largest nonzero $K_{r,s}$ values are the $K_{r,r+1} = K_{r,r-1}$. The values for $K_{r,s}$ fall off with the cube of the distance between the dipoles. Taking a to be equal to b, one finds that the second largest interaction energies are $K_{r,r+3} = K_{r,r-3}$ and these are an order of magnitude smaller than the largest $K_{r,s}$. Consequently, an approximation in which only the exciton-exciton interaction energies involving $K_{r,r+1} = K_{r,r-1}$ is warranted. This yields the two-δ-function form for the exciton-exciton interaction given in Eq. (8). Hence, it has been shown that the system of Fig. 1 implements the Hamiltonian defined by Eqs. (4)–(8) for a controlled phase shifter.

V. DYNAMICS

Considering first a noninteracting case, with $H_I \to 0$, the system is analytically tractable. In this limit, the use of a complete orthonormal set of symmetric and antisymmetric Bloch waves

$$|k, K\rangle = \frac{1}{N_r} \sum_{r,s=0}^{N_r-1} e^{i2\pi K(r+s)/N_r} e^{i2\pi k(r-s)/N_r} B_s^\dagger A_r^\dagger |0\rangle \tag{20}$$

reveals the periodic energy spectrum

$$(H_A + H_B)|k, K\rangle = \left[\hbar(\omega_A + \omega_B) + 2\hbar\omega_{JA}\cos\left(\frac{2\pi}{N_r}(k+K)\right) + 2\hbar\omega_{JB}\cos\left(\frac{2\pi}{N_r}(K-k)\right)\right]|k, K\rangle \equiv \hbar\omega_{k,K}|k, K\rangle. \tag{21}$$

The transmission lines in Eqs. (20) and (21) are now tacitly assumed to be finite, each consisting of N_r chromophores. The correspondence to the Fourier modes of the two lines $K = (k_A + k_B)/2$ indicates that $\hbar K$ denotes the total, average forward momentum, whereas $\hbar k = \hbar(k_A - k_B)/2$ is the (half) momentum discrepancy of the excitons.

Of interest here are the dynamics of two-exciton states in which one exciton resides on each transmission line. The general form of such a state is

$$|\Psi\rangle = \sum_{r,s} \Psi_{r,s} A_r^\dagger B_s^\dagger |0\rangle, \tag{22}$$

with the (noninteracting) dynamics given by

$$|\Psi(t)\rangle = e^{-i(H_A+H_B)t/\hbar}|\Psi\rangle. \tag{23}$$

More generally, the dynamics for the interacting Frenkel exciton system is governed by the Schrödinger equation

$$i\hbar\frac{\partial}{\partial t}|\Psi\rangle = H|\Psi\rangle = (H_A + H_B + H_I)|\Psi\rangle. \tag{24}$$

Substituting Eq. (22) into Eq. (24) for the Hamiltonian of Eqs. (4)–(24) yields

$$\begin{aligned} i\frac{\partial \Psi_{r,s}}{\partial t} &= \omega_A \Psi_{r,s} + \omega_{JA}(\Psi_{r-1,s} + \Psi_{r+1,s}) \\ &\quad + \omega_B \Psi_{r,s} + \omega_{JB}(\Psi_{r,s-1} + \Psi_{r,s+1}) \\ &\quad + \omega_I(\delta_{r,s-1} + \delta_{r,s+1})\Psi_{r,s} \quad \text{for all } r \text{ and } s. \end{aligned} \tag{25}$$

This set of equations is amenable to numerical calculation, especially if periodic boundaries are imposed.

VI. INTERACTING DYNAMICS OF EXCITON COLLISIONS

We consider two-exciton wave packets in collision. Again, each resides in one of two coupled, parallel linear arrays A (top) or B (bottom) labeled in Fig. 1. For simplicity, we consider the case when $\omega_A = \omega_B = \omega_0$ and $\omega_{JA} = \omega_{JB} = \omega_J$. As with Fig. 1, the top A line of N_r total chromophores is indexed by chromophore site r. The wave function is prepared initially as a Gaussian-shaped pulse in the coordinate r, with a speed discussed below. This A-line wave packet is regarded as the faster exciton. The lower B line, indexed by s, has the same initial profile, but is prescribed to either move more slowly in the same direction or move in the opposite direction. If these excitons are initially launched with the slower B-line exciton positioned in advance of the faster one, the faster exciton will overtake the slower one in what we refer to as a rear-end collision. During this collision, the pulses overlap and the interaction of Eq. (7) is nonzero, generally prompting transmitted and reflected waveforms to result. These fractionated waves emanate from the scattering event and they acquire a phase shift in the process. Head-on collisions may also be orchestrated, largely considered below with $K = 0$, a case consisting of wave packets with equal and opposite velocities.

If wave packets on transmission line A are relatively strongly peaked about a particular wave number $k_A = K + k$, they travel with the group velocity [16]

$$v_{gA} = -2\omega_{JA} a \sin k_A = -2\omega_{JA} a \sin(K + k). \tag{26}$$

A similar relation for $v_{gB}(k_B = K - k)$ exists. In this expression, an abbreviation for the wave number has been used, $\frac{2\pi}{N_r} k \to k$, in correspondence with previous convention. The wave packets in either line thus have speeds programmable by wave number.

The dynamics of these collisions are investigated by time stepping a solution to Eq. (25) with an efficient split-step Fourier method. Similar to Eq. (23), writing

$$\Psi_{r,s}(t + \Delta t) = e^{-iH\Delta t/\hbar} \Psi_{r,s}(t) \tag{27}$$

by Taylor's expansion in Δt, it is straightforward to show that

$$\Psi_{r,s}^{(n+1)} = e^{-iH_I \Delta t/2\hbar} e^{-i(H_A + H_B)\Delta t/\hbar} e^{-iH_I \Delta t/2\hbar} \Psi_{r,s}^{(n)} + O(\Delta t^3) \tag{28}$$

for propagation from the nth to the $(n+1)$th time step ($t = n\Delta t$). This method first applies the operator $\exp(-iH_I \Delta t/2\hbar)$, affecting all $(r, s-1)$ and $(r, s+1)$ pairs. Next a fast Fourier transform is applied [20] and the operator $\exp[-i(H_A + H_B)\Delta t/\hbar] = \exp(-i\omega_{k,K}\Delta t)$ from Eq. (21) is simply updated, as it is trivially diagonal in (k, K). Finally, an inverse transform is performed and the operator $\exp(-iH_I \Delta t/2\hbar)$ is again applied in real space. This method has historical roots in solving the Schrödinger equation in other settings [21–23]. For these numeric inquiries, periodic boundary conditions are imposed on the system, which effectively considers a closed-loop system of two A-B coupled lines arranged in a closed ring.

This approach is used to investigate exciton collisions, in both head-on and rear-end configurations, for the case when $\omega_{JA} = \omega_{JB} = \omega_J$. Two head-on collisions are depicted in Fig. 2, where the single-line probabilities are plotted. These are, for example, $P_r(t) = \sum_s |\Psi_{r,s}(t)|^2$, with a similar expression for $P_s(t)$. Figures 2(a) and 2(b) show the excitons of the two lines, A on the left and B on the right, moving with equal speeds in opposite directions, with $K = 0$, $k \approx \pi/8$ ($k_A = 90\pi/721$), and $N_r = 721$ prescribed. Initially displaced, a collision takes place whose most probable location [through the use of Eq. (26)] is indicated with a black dot. Times beyond this point clearly depict partitioned wave packets progressing in accordance with conservation of momentum, i.e., the waveforms continue on with the rates of either of the initial excitons of the lines. Dispersion is mildly evident. It is again worth mentioning that the excitons are sequestered on their individual lines, in which cross hopping in the process of the collision is disallowed.

The trajectories of Fig. 2 are labeled with a convention we utilize below: If the pulses in collision fractionate as they do in Figs. 2(a) and 2(b), they are regarded as consisting of reflected (r) and transmitted (t) portions. The transmitted wave has the same momentum as the initial waveform (i) of the line and the reflected that of the opposite line. Note that the "slow" B-line wave packet (which is traveling left) has a portion of it that is captured and dragged rightward with the momentum of the A line. This portion is yet regarded as a reflected portion of the B waveform.

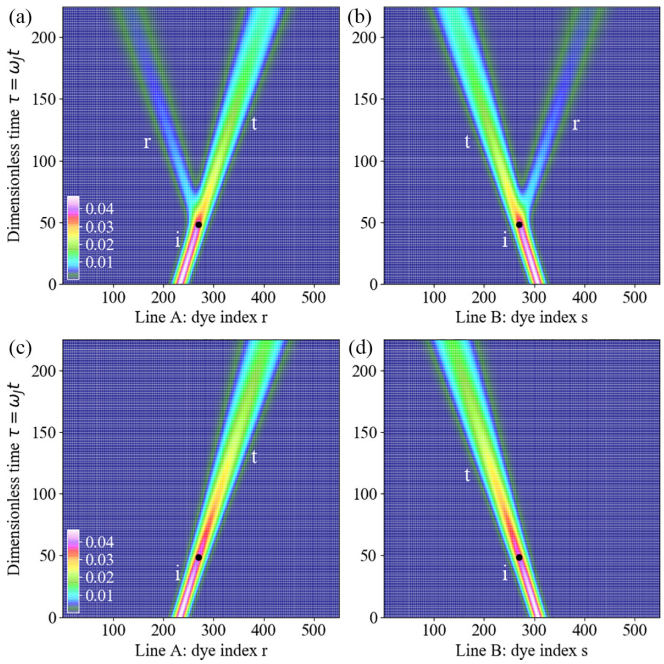

FIG. 2. Two cases of an exciton-exciton head-on collision. Shown is the probability distribution, as a function of time, of (a) a right-propagating exciton (line A) and (b) an initially displaced, left propagating one (line B) in the case of a collision that fractionates the waveforms: $\omega_J/\omega_I = 1/2$ and $k = \pi/8$. Initial A and B wave functions (both denoted by i) are Gaussians of width $\sigma = 12a$, which collide at the ballistic time and location denoted by a black dot, beyond which the waveforms partition into reflected (r) and transmitted (t) portions. (c) and (d) Same collision with a different cross-line exciton-exciton coupling $\omega_J/\omega_I = 0.653\,28$. [See Eq. (49) for a case with no reflections.]

Figures 2(a) and 2(b) depict a case of strong coupling between the lines, with the interaction constant twice the strength of the hopping rate of the lines. This results in about 24% reflection of the excitons. If this interaction is weakened, the portion reflected diminishes and, for a special value, it vanishes altogether. This case is shown in 2(c) and 2(d) and discussed in more detail in Sec. VII.

The second collision considered is that of the rear-end collision, with a fast exciton catching up to and then overtaking a slower one. This case is illustrated in Fig. 3, with the A-line signal encountering a slower exciton placed initially ahead of it on the B line. Figures 3(a) and 3(b) again illustrate a strongly coupled case with emanating reflections ($\omega_J/\omega_I = 2/3$) from the overtaking collision, whose most probable time and position are again marked with a black dot. Similar to Fig. 2, upon weakening the exciton-exciton interaction, a no-reflection case is found once again and shown in Figs. 3(c) and 3(d).

We note in passing that the transmission lines in both Figs. 2 and 3 are larger than the range shown (both have $N_r = 721$), so at late times the signals do not wrap through the periodic edge of the abscissa. This has been chosen for clarity of presentation.

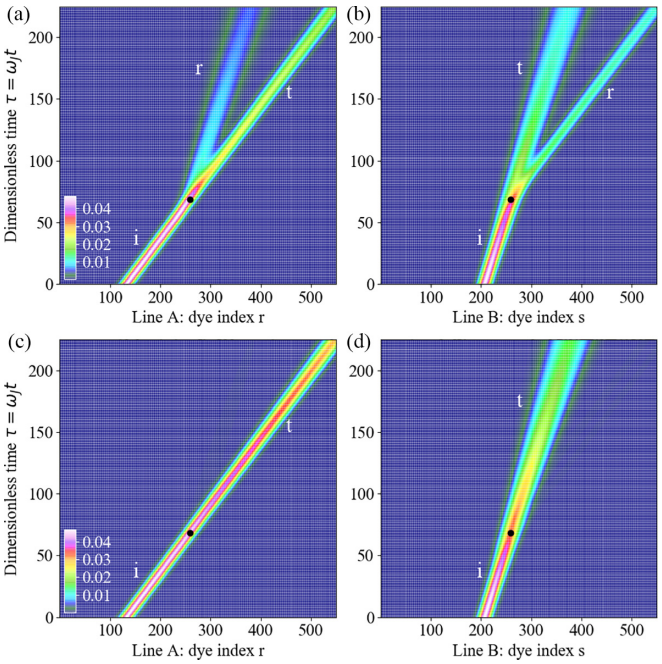

FIG. 3. Exciton probability distributions as a function of time for the case of an exciton-exciton collision in which a fast exciton on line A overtakes a slow one on line B. Reflections are present in (a) and (b) ($\omega_J/\omega_I = 2/3$, $K = \pi/4$, $k = \pi/8$, and $|R|^2 \approx 0.364$), whereas only transmitted (t) signals result in the collision in (c) and (d) ($\omega_J/\omega_I = 0.923\,88$, $K = \pi/4$, and $k = \pi/8$). See the text for details.

VII. ANALYTICAL RESULTS

Again restricting our analysis to equal transition energies $\omega_A = \omega_B = \omega_0$ and equal hopping rates $\omega_{JA} = \omega_{JB} = \omega_J$, the dispersion relation of Eq. (21) reduces to

$$\omega_E = 2\omega_0 + 4\omega_J \cos(K)\cos(k). \tag{29}$$

With the periodicity of the system, the Bloch-form energy eigenstates (20) have the general form

$$\Psi_{r,s} = e^{-i\omega_E t} e^{iK(r+s)} \psi_{r-s}. \tag{30}$$

Excitons in pairs are noninteracting except when they are within a lattice unit of each other, and apart from this they act as free distinguishable particles. Hence, when $|r-s| > 1$, one expects ψ_{r-s} to have the form of the energy eigenstate of a free particle, $e^{\pm ik(r-s)}$. Introducing $v = r - s$, we thus impose the ansatz

$$\psi_v = A_+ e^{ikv} + A_- e^{-ikv} \quad \text{for } v < -1, \tag{31}$$

$$\psi_{-1} = B, \tag{32}$$

$$\psi_0 = C, \tag{33}$$

$$\psi_1 = D, \tag{34}$$

$$\psi_v = E_+ e^{ikv} + E_- e^{-ikv} \quad \text{for } v > 1. \tag{35}$$

For Eqs. (31) and (35) to satisfy Eq. (25) generally, the dispersion relation of Eq. (29) must hold, which can be demonstrated by direct substitution. Substitution of Eqs. (31)–(35) into Eq. (25) using Eq. (30) yields five equations linear in $(A_\pm, B, C, D, E_\pm)$. These equations can be solved to express A_-, B, C, D, and A_- in terms of A_+ and E_-. In particular, one finds

$$\begin{bmatrix} E_+ \\ A_- \end{bmatrix} = \begin{bmatrix} T & R \\ R & T \end{bmatrix} \begin{bmatrix} A_+ \\ E_- \end{bmatrix}, \tag{36}$$

where T and R are the transmission and reflection coefficients of the scattering produced by the exciton-exciton interaction. These coefficients are given by

$$T = \frac{-4i\omega_J^2 \cos^2(K)\sin(k)}{\omega_I^2 e^{2ik}\cos(k) - 2\omega_I\omega_J\cos(K) - 4i\omega_J^2\cos^2(K)\sin(k)} \tag{37}$$

and

$$R = \frac{\omega_I[2\omega_J\cos(K)\cos(2k) - \omega_I\cos(k)]}{\omega_I^2 e^{2ik}\cos(k) - 2\omega_I\omega_J\cos(K) - 4i\omega_J^2\cos^2(K)\sin(k)}. \tag{38}$$

The conservation of energy and the conservation of probability both require that the transformation (36) must be unitary. Hence, T and R satisfy the useful relations

$$|T|^2 + |R|^2 = 1 \tag{39}$$

and

$$TR^* + RT^* = 0. \tag{40}$$

VIII. OPERATING POINTS

For the controlled phase shifter to function properly no reflection (backscattering) must occur when the two excitons interact, that is, $R = 0$. From Eq. (38) one finds that this condition is met when the exciton-exciton interaction energy $\hbar\omega_I$ is zero. In this case, Eq. (36) becomes

$$\begin{bmatrix} E_+ \\ A_- \end{bmatrix} = \begin{bmatrix} 1 & 0 \\ 0 & 1 \end{bmatrix} \begin{bmatrix} A_+ \\ E_- \end{bmatrix}. \tag{41}$$

From Eq. (38) one also finds that the condition $R = 0$ can still be met when the exciton-exciton interaction energy is not zero provided,

$$\cos(K) = \frac{\omega_I}{2\omega_J}\left(\frac{\cos(k)}{\cos(2k)}\right). \tag{42}$$

In this case Eq. (36) becomes

$$\begin{bmatrix} E_+ \\ A_- \end{bmatrix} = \begin{bmatrix} e^{i4k} & 0 \\ 0 & e^{i4k} \end{bmatrix} \begin{bmatrix} A_+ \\ E_- \end{bmatrix}. \tag{43}$$

Comparing Eqs. (41) and (43), one sees that a phase shift of $\phi = 4k$ is produced by the exciton-exciton coupling as one exciton overtakes the other.

A. Example operating points

Here example operating points are exhibited for the case when the controlled phase shifter induces a phase shift of $\pi/2$. To achieve this, it is evident from Eq. (43) that one must have

$$k = \frac{\pi}{8}. \tag{44}$$

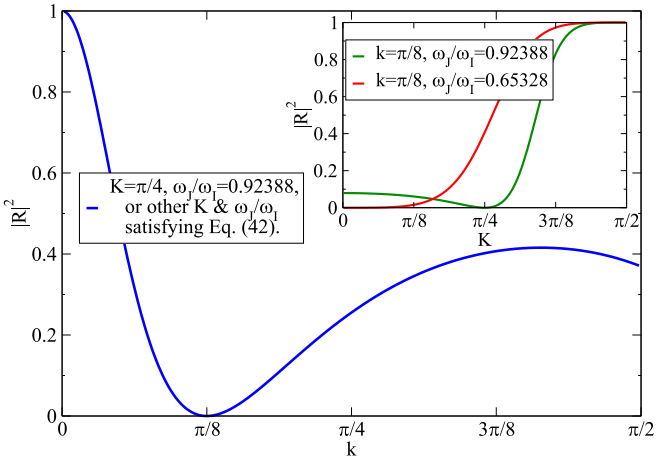

FIG. 4. Reflection probability $|R|^2$ for the interaction coupling ratio (47) with prescribed $K = \pi/4$ and varying k. The inset depicts $|R|^2$ for the same interaction coupling ratio but with fixed $k = \pi/8$ and varying total average momentum K (in green). A second case is also shown (see the text for details).

Substituting this into Eq. (42) yields

$$\cos(K) = \frac{1}{2}\sqrt{\frac{\sqrt{2}+1}{\sqrt{2}}}\frac{\omega_I}{\omega_J}. \tag{45}$$

Choosing

$$K = \frac{\pi}{4} \tag{46}$$

yields

$$\frac{\omega_J}{\omega_I} = \sqrt{\frac{\sqrt{2}+1}{2\sqrt{2}}} = 0.923\,88. \tag{47}$$

Operated in this mode, the two excitons have different wave vectors. The slower one has a wave vector of $k_B = K - k = \pi/8$, whereas the faster one has a wave vector of $k_A = K + k = 3\pi/8$. The wave packet of the slower exciton is thus able to overtake that of the faster one in a rear-end collision, and this is the case depicted in Fig. 3. Complete passthrough of the faster wave packet through the slower one and proper operation of the controlled phase shifter is achieved when the ratio of the exciton hopping energy to the exciton-exciton interaction energy is given by Eq. (47). This requires chromophores for which the dipole-dipole interactions (2) and (3) can be engineered to be comparable. Transition dipoles of strongly absorbing fluorescent organic dyes are in the 16 D range [24]. Engineering dyes with large-difference static dipoles has received less attention, but theoretical work [25] indicates that these can be as large as 20 D. The ability to control the strength of the $J_{r,s}$ and the $K_{r,s}$ by chromophore separation or orientation should enable the condition (47) to be met.

The reflection probability $|R|^2$ in the vicinity of the passthrough optimum is shown in Fig. 4. The reflection probability for systems with average total momentum $K = \pi/4$ is shown as a function of the momentum discrepancy of the respective excitons k, including the spurious limit $k \to 0$ that has never- or always-overlapping or interacting pulses. Reflections wane from this point with growing k to disappear at the operating point for the overtaking collision described by Eqs. (44), (46), and (47).

Equation (42) may be written as $X^*/\cos(K) = 2\cos(2k)/\cos(k)$, with $X^* = \omega_I/\omega_J$. When this condition is satisfied (a necessary condition for no backscattering) reflections $|R|^2(k)$ for any k are invariant under the transformation $K_1 \to K_2$, so long as $X_1^*/\cos K_1 \to X_2^*/\cos K_2$. Consequently, the condition for vanishing reflections in these collisions is also invariant under this transformation, provided the momentum difference is maintained at $k = \pi/8$. This is also to say, for *any* average net momentum $0 \geqslant K < \pi/2$ among colliding excitons that have a maintained $k = \pi/8$ momentum difference, a zero-reflection point exists that is given by the conditions of Eq. (45).

Shown in the Fig. 4 inset is the reflection probability when $k = \pi/8$ is prescribed, but with varying K, for two values of ω_J/ω_I $(=1/X^*)$. The green profile depicts the overtaking collision operating point above, which has $R = 0$ at $K = \pi/4$. Pulling away from $K = \pi/4$, the condition for zero reflections is met in accordance with the invariance mentioned above. A second case with $|R|^2 = 0$ at $K = 0$ is shown in red. This case has

$$K = 0 \tag{48}$$

and Eq. (45) yields

$$\frac{\omega_J}{\omega_I} = \frac{1}{2}\sqrt{\frac{\sqrt{2}+1}{\sqrt{2}}} = 0.653\,28. \tag{49}$$

Operated in this mode, one exciton travels with the momentum $K - k = -k$ while the other travels with the momentum $K + k = k$. The two excitons thus travel in opposite directions and engage in a head-on collision, exactly the circumstance illustrated in Fig. 2. The exciton wave packets pass through each other without backscattering and with proper operation as a controlled phase shifter when the ratio of ω_J to ω_I is given by Eq. (49). Although this mode of operation requires a larger ω_I relative to ω_J, it offers several advantages: The energy of both excitons is the same and the transmission-line length can be shorter, as it need only be twice the length of the exciton wave packet.

The phase shifts acquired in the collisions are shown in Fig. 5. The panels and color of this figure correspond to those of Fig. 4. The phase as a function of k for all K and ω_J/ω_I satisfying Eq. (42) is shown in the main panel and that for variable K, with $k = \pi/8$, in the inset. The no backscattering invariance with X and K again reduces all phases to a single trajectory in k shown in the main panel. Variations from the desired phase $\phi = \pi/2$ are evident with changes from $k = \pi/8$ or $K = \pi/4$.

B. Bandwidth tolerance

The performance of the controlled phase shifter will degrade when operated away from its operating point. This limits the bandwidth of the device and sets the accuracy with which the chromophore positions and orientations must be maintained to achieve a desired level of performance. A demanding application of a controlled phase shifter would

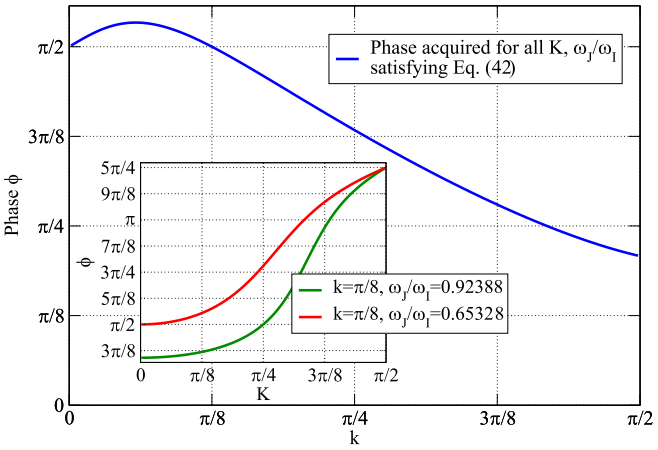

FIG. 5. Phase shift acquired in exciton-exciton collisions for set K and varying k for the interaction coupling ratio (47). The inset shows the phase shift for set $k = \pi/8$ but varying K at the interaction coupling ratios of Eqs. (47) and (49) (green and red, respectively).

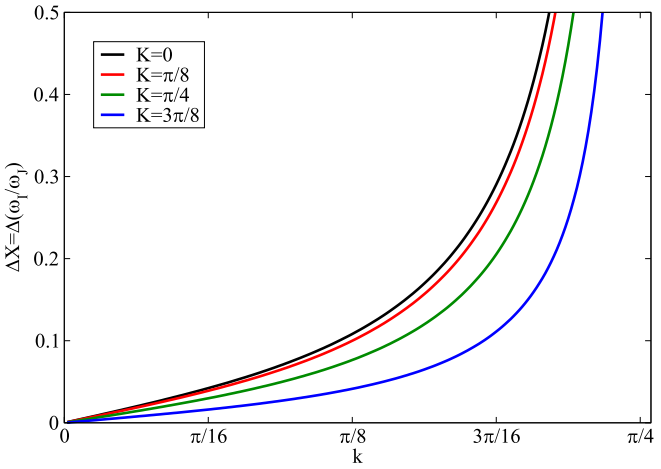

FIG. 6. Tolerance estimates for the interaction energy ratio $X = \omega_I/\omega_J$ requiring no greater than 1% reflection. The case $K = 0$ has excitons traveling from opposite directions into a head-on collision, whereas $K > 0$ has a fast pulse of momentum $\hbar(K + k)$ overtaking a slow one with $\hbar(K - k)$. A greater momentum discrepancy $\hbar k$ among the pulses enables a less stringent requirement for the couplings ΔX.

be its use as a component of a quantum gate for quantum computation that is scalable and universal. In this application, scalability can be achieved through quantum error correction if the error rate per gate is reduced below a certain threshold value [26,27]. Error correction schemes have been devised for which the threshold error rate is about 1% per gate.

Here the tolerance in $X = \omega_I/\omega_J$ is considered. Reflections from Eq. (38) may be simply written

$$|R|^2 = \frac{1}{1 + \left(\frac{4\cos^2(K)\sin(k)}{X[X\cos(k) - 2\cos(K)\cos(2k)]}\right)^2}. \tag{50}$$

Expansions in $|R|^2$ about the zero-reflection point of Eq. (42), $X^* = 2\cos(K)\cos(2k)/\cos(k)$, yield $|R|^2 \approx c\Delta X^2$ for small $\Delta X = X - X^*$, with $c = \cos^2(k)\cot^2(2k)\sec^2(K)$. Requiring just 1% tolerance in reflections, this threshold for the tunable interaction ratio $\Delta X \approx \sqrt{0.01/c}$ is displayed in Fig. 6. For pulses propagating in opposite directions, with total average momentum $K = 0$, this tolerance is the most lenient of the profiles. A smaller window of precision in ΔX is necessary to achieve the same minimal reflection result for cases with $K > 0$, in which fast excitons overtake slower ones. In these rear-end collisions, as the momentum discrepancy $\hbar k$ in the two lines grows, an ever speedier fast pulse overtakes a slower slow exciton (i.e., cases with greater k values but equal K's), and the required window of precision in ΔX increases, becoming less stringent. It is the longer duration of pulse overlap during collisions that degrades performance.

The analysis presented has employed the nearest-neighbor approximation for the intra-transmission-line exciton exchange interactions. Including more distant neighbor interactions will yield a more complicated dispersion relation than that of Eq. (29). The analysis has also neglected the more distant inter-transmission-line exciton-exciton interactions. The inclusion of the neglected interactions will alter the functional dependence of the transmission and reflection coefficients on k and K, but the existence of operating points where total destructive interference of the backscattered waves occurs resulting in no backreflection is still expected. The value of ω_J/ω_I at which the phase shifts is $\pi/2$, for the controlled phase shifter will differ from those given in Eqs. (47) and (49).

IX. QUANTUM GATES

The controlled phase shifter enables the implementation of an exciton-based controlled-phase (CPHASE) gate as shown in Fig. 7(a). The symbol for a controlled-phase gate inducing a phase shift of ϕ is shown in Fig. 7(b). The CPHASE gate in conjunction with single-qubit basis-change gates and phase gates enable universal quantum computation. In the scheme shown in Fig. 7(a), a dual-rail implementation of a qubit is employed. In this representation, the exciton is carried by a pair of transmission lines. The qubit consists of the probability amplitudes with which the exciton resides on either of the two transmission lines. In Fig. 7(a) the qubit q_0 occupies the upper two transmission lines. The upper of these two lines is assigned as the line on which the exciton resides when the

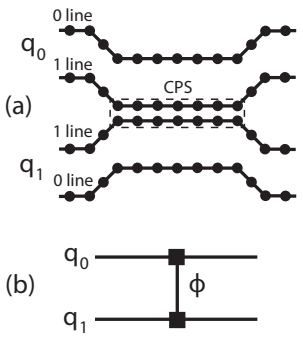

FIG. 7. (a) Schematic of an exciton-based controlled-phase gate employing a controlled phase shifter (CPS). See the text for details. (b) Symbol for a CPHASE gate inducing a phase shift of ϕ. This gate is denoted by $G_{\text{CPHASE}}(\phi)$.

value of q_0 is logical zero (0 line). The lower of these two lines is assigned as the line on which the exciton resides when the value of q_0 is a logical one (1 line). The qubit q_1 is carried by the lower transmission-line pair and, to maintain standard notation, the upper of these transmission lines is the logical 1 line whereas the lower is the logical zero line. A phase shift due to excision-exciton interaction in the controlled phase shifter element occurs only when an exciton is present on the 1 line of q_0 and the 1 line of q_1. Denoting the state for which q_0 has the logical value x and the state for which q_1 has the logical value y by $|xy\rangle$, the $G_{\text{CPHASE}}(\phi)$ gate performs the transformations

$$|00\rangle \to |00\rangle, \quad |01\rangle \to |01\rangle,$$
$$|10\rangle \to |10\rangle, \quad |11\rangle \to e^{i\phi}|11\rangle,$$

that is, the CPHASE gate performs the unitary transformation

$$G_{\text{CPHASE}}(\phi) = \begin{bmatrix} 1 & 0 & 0 & 0 \\ 0 & 1 & 0 & 0 \\ 0 & 0 & 1 & 0 \\ 0 & 0 & 0 & e^{i\phi} \end{bmatrix}. \tag{51}$$

Equations (42) and (43) enable the engineering of a CPHASE gate with a phase shift in the range $-\pi < \phi < \pi$ and the design of controlled phase shifters providing a phase shift of $\pi/2$ has been shown with two examples in Sec. VIII. A CPHASE gate with a phase shift of π is a useful element in the implementation of quantum logic circuits, but the realization of a phase shift of π is problematic for the controlled phase shifter we have presented. By routing the transmission lines carrying the output of one controlled $\pi/2$ phase shifter to the input of a second such phase shifter, a controlled phase shift of π is achieved. This requires that the lengths of the transmission lines carrying the excitons from the first to the second controlled phase shifter be chosen so that the exciton wave packets collide within the second phase shifter. The combined system can then function as the controlled π phase shifting element of a $G_{\text{CPHASE}}(\pi)$ gate.

An advantage of the dual-rail representation is that single-qubit gates such as phase gates and basis-change gates can be simply implemented. These together with the CPHASE gate form a complete set of gates for universal quantum computation. Phase gates can be implemented as propagation delays through change of length, optical transition frequency, or exciton hopping frequency in a portion of the transmission line. As shown in Fig. 8(a), a basis-change gate can be implemented by bringing a portion of two transmission lines carrying a qubit sufficiently close together that exciton exchange occurs between the transmission lines as indicated by the black edges between the nodes. The design of such gates has been discussed by Yurke and Kuang [17]. By a judicious choice of the exciton exchange couplings between chromophores, which can be engineered by adjusting chromophore spacing or orientation, any basis transformation can be realized. Of particular interest here is the Hadamard gate represented by a box with the letter H in Figs. 8(b) and 8(d). This is a

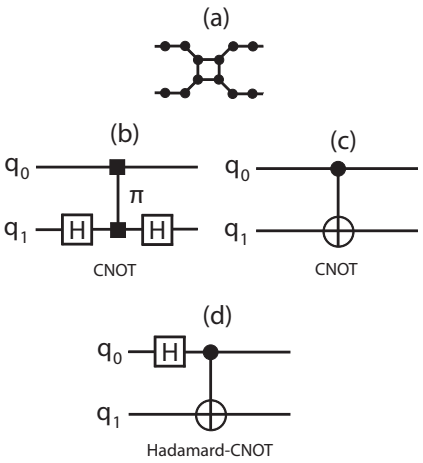

FIG. 8. (a) Schematic of a basis-change gate. (b) A CNOT gate implemented using two Hadamard gates and a $G_{\text{CPHASE}}(\pi)$ gate. (c) Symbol for a CNOT gate. (d) Hadamard CNOT gate.

basis-change gate performing the transformation

$$\frac{1}{\sqrt{2}}\begin{bmatrix} 1 & 1 \\ 1 & -1 \end{bmatrix} \tag{52}$$

on the logical 0 and logical 1 basis of the qubit. Figure 8(b) shows how a CNOT gate can be implemented using two Hadamard gates and a $G_{\text{CPHASE}}(\pi)$ gate. The symbol for a CNOT gate is shown in Fig. 8(c). As an example of a potentially useful exciton circuit, Fig. 8(d) shows a Hadamard CNOT gate implemented by inserting a Hadamard gate in the control line q_0 of a CNOT gate. This gate can serve as a source of maximally entangled excitons. In particular, this gate converts the state $|00\rangle$, in which the excitons of qubits q_0 and q_1 both reside on their respective logical zero lines, into the Bell state

$$|\text{Bell}\rangle = \frac{|00\rangle + |11\rangle}{\sqrt{2}}, \tag{53}$$

which is a superposition state in which, upon exiting the gate, either each exciton resides on its logical 0 line or each exciton resides on its logical 1 line. Because product states, such as $|00\rangle$, are easier to prepare by laser excitation of the ends of transmission lines than Bell states, the Hadamard CNOT gate can serve as a means of converting these states into maximally entangled exciton states.

Since a computation architecture has been envisioned where each qubit is carried by a transmission-line pair that passes through various gates in which transmission-line segments are brought close together to enable one-qubit or two-qubit operations, an estimate of the circuit complexity that is possible with currently available chromophores is obtained by considering the distance an exciton can travel along its transmission-line pair before decoherence sets in. Due to coupling of excitons with molecular vibrations, the decoherence time for typical chromophore consisting of an organic dye is generally in the tens of femtoseconds. Here, for the coherence lifetime, we use the 60 fs measured by Duan *et al.* [28] for the chromophores of the Fenna-Matthews-Olson protein. The travel distance of the exciton is obtained by multiplying the coherence time by the group velocity of

the transmission line. Considering Eq. (26), an estimate of the group velocity is provided by $v_g = 2\omega_J a$. Exciton hopping energies in excess of 100 meV are commonly exhibited in chromophore aggregates yielding a hopping frequency of 1.5×10^{14} s^{-1} and the speed with which an exciton moves of 3×10^{14} s^{-1} per lattice spacing unit. The exciton thus travels nine lattice units during the coherence time, indicating that practical Frenkel exciton-based quantum gates and networks would be rather limited in size. The coherence time is expected to lengthen at low temperatures and chromophores with reduced exciton-vibration coupling may yet be identified, thus offering hope that larger gate networks will be possible.

Having indicated that chromophores can be arranged in networks that function as quantum gates and that can be cascaded to implement quantum computation circuits, an issue still to be addressed is initialization and qubit readout. The excitons can be launched by providing the input end of one transmission line, of each transmission-line pair, with an antenna that is able to absorb a photon and convert it into an exciton with near unit quantum efficiency. This antenna could consist of a single chromophore or a cluster of chromophores. The excitation of chromophores other than those associated with the antenna can be avoided by proper orientation of the chromophores with respect to the direction of polarization of the excitation light. For example, light polarized along the y axis in Fig. 1 will not excite the chromophores of this transmission-line system because the polarization is orthogonal to the orientation of the transition dipoles. At least one chromophore of the antenna complex would have a transition dipole that is not orthogonal to the direction of light polarization. By simultaneously applying a single-photon light pulse to each antenna the input end of each transmission line could be prepared with a qubit having the truth value of logical 1. This multiqubit input state would then be processed by the chromophore network to carry out the unitary transformation that performs the desired quantum computation. Readout can be carried out in an analogous manner in which the output end of each transmission line is provided with an antenna that converts an exciton into a photon. If each transmission line is terminated at a different length at the output end, the time at which each photon is emitted will differ, thereby enabling a time multiplexed readout coded in the arrival time of each photon at a photodetector.

X. CONCLUSION

Controlled gates such as a controlled-NOT gate are essential for universal quantum computation. Such gates can be constructed by employing a controlled phase shifter element. In one of their embodiments of a controlled phase shifter element, for the case when the particles are distinguishable, Childs *et al.* [16] employed a two-δ-function particle-particle interaction to implement a controlled phase shifter element. This raises the issue whether such an interaction can be engineered in a physical system. Here we have shown that a two-δ-function interaction can be implemented in a pair of transmission lines constructed by employing at least two types of chromophores: one for which the transition dipole and the difference static dipole are parallel and the other for which the transition dipole and difference static dipole are not parallel but preferably orthogonal. Organic chromophore-containing dye molecules with these properties do exist [19]. The chromophores are arranged such that the transition dipoles of one transmission line are orthogonal to those of the other. In this configuration, exciton transfer from one transmission line to the other is prevented because the inter-transmission-line hopping interactions are zero. The difference static dipoles are arranged, however, in an alternating manner for which the nearest-neighbor difference static dipole-dipole coupling is zero. This leaves the next-nearest-neighbor inter-transmission-line dipole-dipole couplings as the dominant exciton-exciton interaction, thereby implementing a two-δ-function Hubbard interaction. This two-transmission-line implementation of a controlled phase shifter is well suited for quantum gate implementation employing a dual-rail architecture in which a qubit is encoded by the probability amplitudes existing on one or the other of two transmission lines.

DNA-based self-assembly currently offers the best possibility for implementing Frenkel exciton-based transmission lines and gates through chromophore organization. Organic dyes, however, are strongly coupled to the environment through the interaction of vibrational degrees of freedom with the electronic degrees of freedom of their chromophores, which leads to short exciton coherence times. The extent to which chromophores can be engineered to lengthen these times is an interesting question [13], as long exciton coherence times would enable the implementation of various coherent exciton-based devices, including entangled exciton sources, with potential applications in optical information processing and, as shown here, potentially universal quantum computation.

ACKNOWLEDGMENTS

The linkage to universal quantum computation and demonstration of how specific required quantum gates for computing could be implemented using Frenkel excitons was supported by the U.S. Department of Navy, Office of Naval Science via Award No. N00014-19-1-2615. The demonstration of how implementation of a CNOT gate could be used to generate maximally entangled two-exciton states was supported by the U.S. Department of Energy (DOE), Office of Basic Energy Sciences, Materials Sciences and Engineering Division and DOE's Established Program to Stimulate Competitive Research (EPSCOR) program via Award No. DE-SC0020089.

[1] X. Yan, S. Huang, Y. Wang, Y. Tang, and Y. Tian, Nano Mater. **10**, 2047 (2020).

[2] Y. Chen, W. Sun, C. Yang, and Z. Zhu, ACS Appl. Bio Mater. **3**, 2805 (2020).

[3] S. Buckhout-White, C. M. Spillmann, W. R. Algar, A. Khachatrian, J. S. Melinger, E. R. Goldman, M. G. Ancona, and I. L. Medintz, Nat. Commun. **5**, 5615 (2014).
[4] B. Albinsson, J. K. Hannestad, and K. Börjesson, Coord. Chem. Rev. **256**, 2399 (2012).
[5] W. Su, V. Bonnard, and G. A. Burley, Chem. Eur. J. **17**, 7982 (2011).
[6] J. S. Huff, D. B. Turner, O. A. Mass, L. K. Patten, C. K. Wilson, S. K. Roy, M. S. Barclay, B. Yurke, W. B. Knowlton, P. H. Davis, and R. D. Pensack, J. Phys. Chem. B **125**, 10240 (2021).
[7] R. S. Rukin, K. G. Komarova, B. Fresch, E. Collini, and F. Remacle, Phys. Chem. Chem. Phys. **22**, 7516 (2020).
[8] J. S. Huff, P. H. Davis, A. Christy, D. L. Kellis, N. Kandadai, Z. S. D. Toa, G. D. Scholes, B. Yurke, W. B. Knowlton, and R. D. Pensack, J. Phys. Chem. Lett. **10**, 2386 (2019).
[9] B. L. Cannon, D. L. Kellis, L. K. Patten, P. H. Davis, J. Lee, E. Graugnard, B. Yurke, and W. B. Knowlton, J. Phys. Chem. A **121**, 6905 (2017).
[10] L. I. Markova, V. L. Malinovskii, L. D. Patsenker, and R. Häner, Chem. Commun. **49**, 5298 (2013).
[11] H. Asanuma, T. Fujii, T. Kato, and H. Kashida, J. Photochem. Photobiol. C **13**, 124 (2012).
[12] M. A. Castellanos and A. P. Willard, Phys. Chem. Chem. Phys. **23**, 15196 (2021).
[13] M. A. Castellanos, A. Dodin, and A. P. Willard, Phys. Chem. Chem. Phys. **22**, 3048 (2020).
[14] D. Abramavicius, B. Palmieri, and S. Mukamel, Chem. Phys. **357**, 79 (2009).
[15] D. Abramavicius, Europhys. Lett. **101**, 57007 (2013).
[16] A. M. Childs, D. Gosset, and Z. Webb, Science **339**, 791 (2013).
[17] B. Yurke and W. Kuang, Phys. Rev. A **81**, 033814 (2010).
[18] O. Kühn, T. Renger, and V. May, Chem. Phys. **204**, 99 (1996).
[19] C. van Galen, D. T. Barnard, and R. J. Stanley, J. Phys. Chem. B **124**, 11835 (2020).
[20] M. Frigo and S. G. Johnson, *Proceedings of the 1998 IEEE International Conference on Acoustics, Speech and Signal Processing* (IEEE, Piscataway, 1998), Vol. 3, pp. 1381–1384.
[21] J. A. Fleck, J. Morris, and M. Feit, Appl. Phys. **10**, 129 (1976).
[22] R. H. Hardin and F. D. Tappert, SIAM Rev. (Chronicle) **15**, 423 (1973).
[23] M. D. Feit, J. A. Fleck, Jr., and A. Steiger, J. Comput. Phys. **47**, 412 (1982).
[24] A. Biaggne, W. B. Knowlton, B. Yurke, J. Lee, and L. Li, Molecules **26**, 524 (2021).
[25] D. Jacquemin, J. Chem. Theory Comput. **12**, 3993 (2016).
[26] A. M. Stephens, Phys. Rev. A **89**, 022321 (2014).
[27] A. G. Fowler, M. Mariantoni, J. M. Martinis, and A. N. Cleland, Phys. Rev. A **86**, 032324 (2012).
[28] H.-G. Duan, V. I. Prokhorenko, R. J. Cogdell, K. Ashraf, A. L. Stevens, M. Thorwart, and R. D. Miller, Proc. Natl. Acad. Sci. USA **114**, 8493 (2017).